Supplementary Materials for

Anatomical evidence for parasympathetic innervation of the renal vasculature and pelvis

Correspondence to: xlliu@mail.hust.edu.cn and sqzeng@mail.hust.edu.cn

Table of Contents

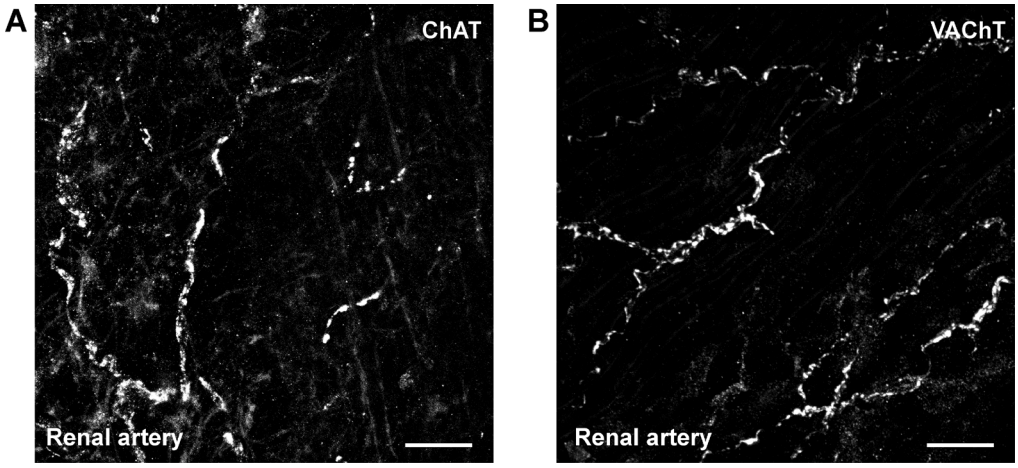

Supplemental Figure 1. ChAT and VAChT immunoreactivity nerve fibers traveled with the renal artery of C57BL/6 mouse. (A) Representative image of the renal artery from a C57BL/6J mouse, stained for ChAT (white). Scale bar, 20 μm. **(B)** Representative image of the renal artery from a C57BL/6J mouse, stained for VAChT (white). Scale bar, 20 μm.

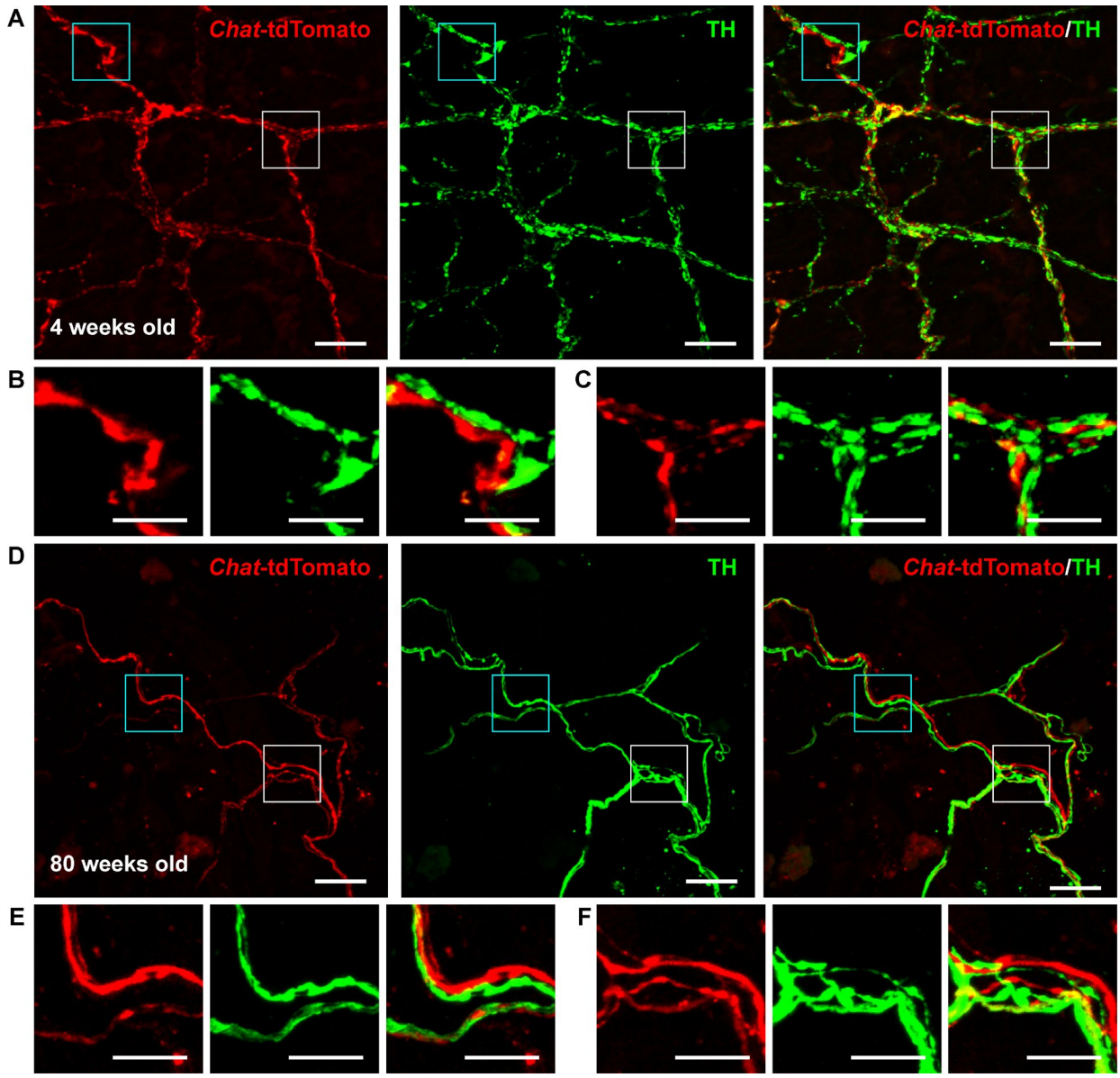

Supplemental Figure 2. Anatomical relationship between cholinergic and catecholaminergic nerve fibers around the renal artery at different ages. (A) Representative images of renal arteries from 4 weeks old *Chat-ires-Cre*:Ai14 mice, stained for TH (green). Note the separation between tdTomato-positive nerve fibers (red) and TH-immunoreactive nerve fibers (green). Scale bars, 20 μm. **(B)** Higher magnification images of the blue light box regions in (A). Scale bars, 10 μm. **(C)** Higher magnification images of the white box regions in (A). Scale bars, 10 μm. **(D)** Representative images of renal arteries from 80 weeks old *Chat-ires-Cre*:Ai14 mice, stained for TH (green). Note the separation between tdTomato-positive nerve fibers (red) and TH-immunoreactive nerve fibers (green). Scale bars, 20 μm. **(E)** Higher magnification images of the blue light box regions in (D). Scale bars, 10 μm. **(F)** Higher magnification images of the white box regions in (D). Scale bars, 10 μm.

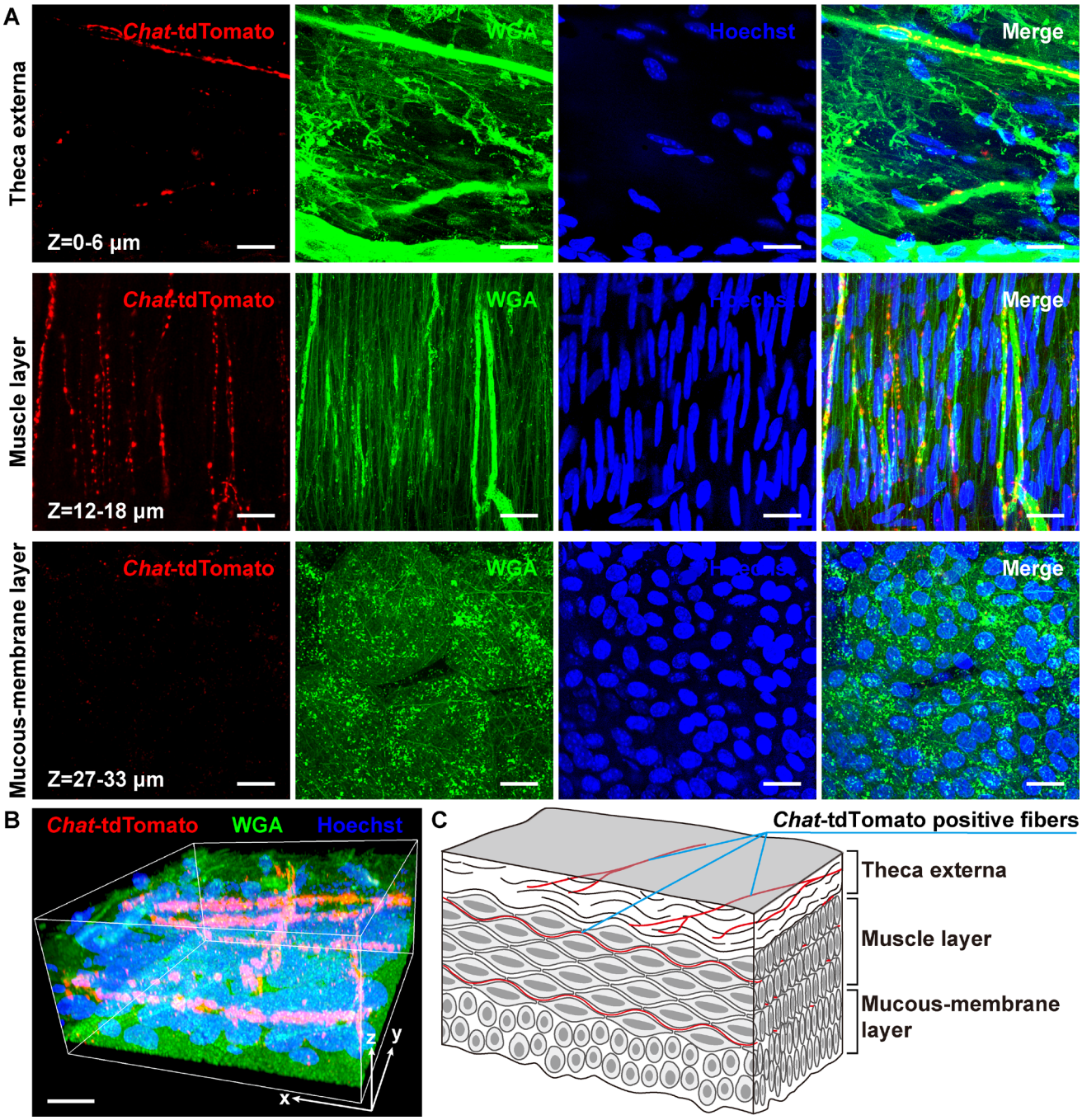

Supplemental Figure 3. The *Chat*-tdTomato positive fibers located in the pelvis wall. (A) Confocal images showing the theca externa, muscle layer, and mucous-membrane layer of renal pelvis wall from *Chat-ires-Cre*:Ai14 mice, stained for WGA (green) and Hoechst 33258 (blue). Note the distribution of *Chat*-tdTomato positive fibers in the theca externa and muscle layer. Scale bars, 20 μm. **(B)** A three-dimensional view of renal pelvis wall in a *Chat-ires-Cre*:Ai14 mice, stained for WGA (green) and Hoechst 33258 (blue). Scale bar, 15 μm. **(C)** A schematic representation of the location of *Chat*-tdTomato positive fibers in the renal pelvis wall.

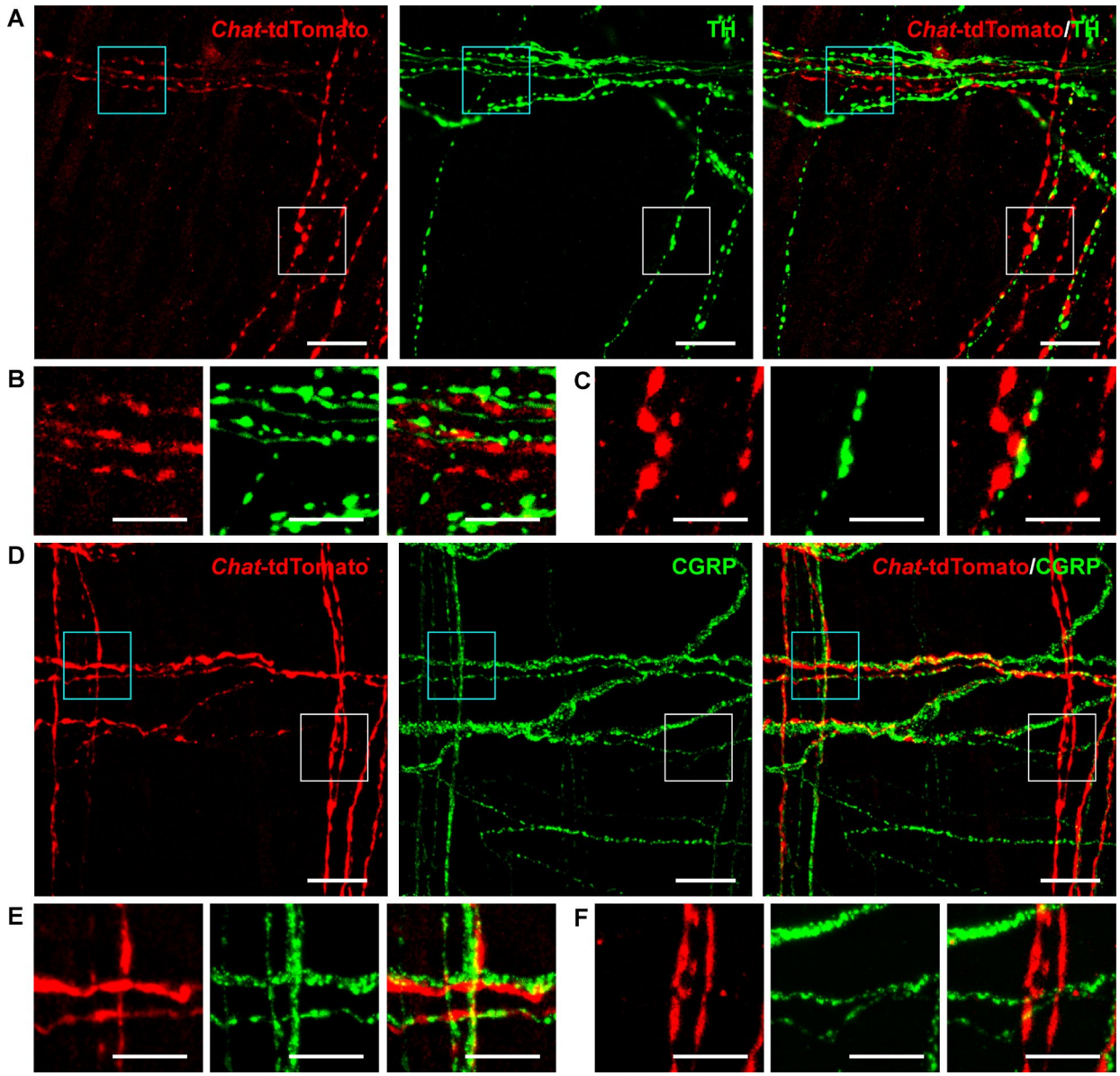

Supplemental Figure 4. Anatomical relationship between cholinergic, sympathetic, and sensory nerve fibers in the renal pelvis wall. (A) Representative images of renal pelvis walls from adult *Chat-ires-Cre*:Ai14 mice, stained for TH (green). Note the separation between tdTomato-positive nerve fibers (red) and TH-immunoreactive nerve fibers (green). Scale bars, 20 μm. **(B)** Higher magnification images of the light blue box regions in (A). Scale bars, 10 μm. **(C)** Higher magnification images of the white box regions in (A). Scale bars, 10 μm. **(D)** Representative images of renal pelvis walls from adult *Chat-ires-Cre*:Ai14 mice, stained for CGRP (green). Note the separation between tdTomato-positive nerve fibers (red) and CGRP-immunoreactive nerve fibers (green). Scale bars, 20 μm. **(E)** Higher magnification images of the light blue box regions in (D). Scale bars, 10 μm. **(F)** Higher magnification images of the white box regions in (D). Scale bars, 10 μm.

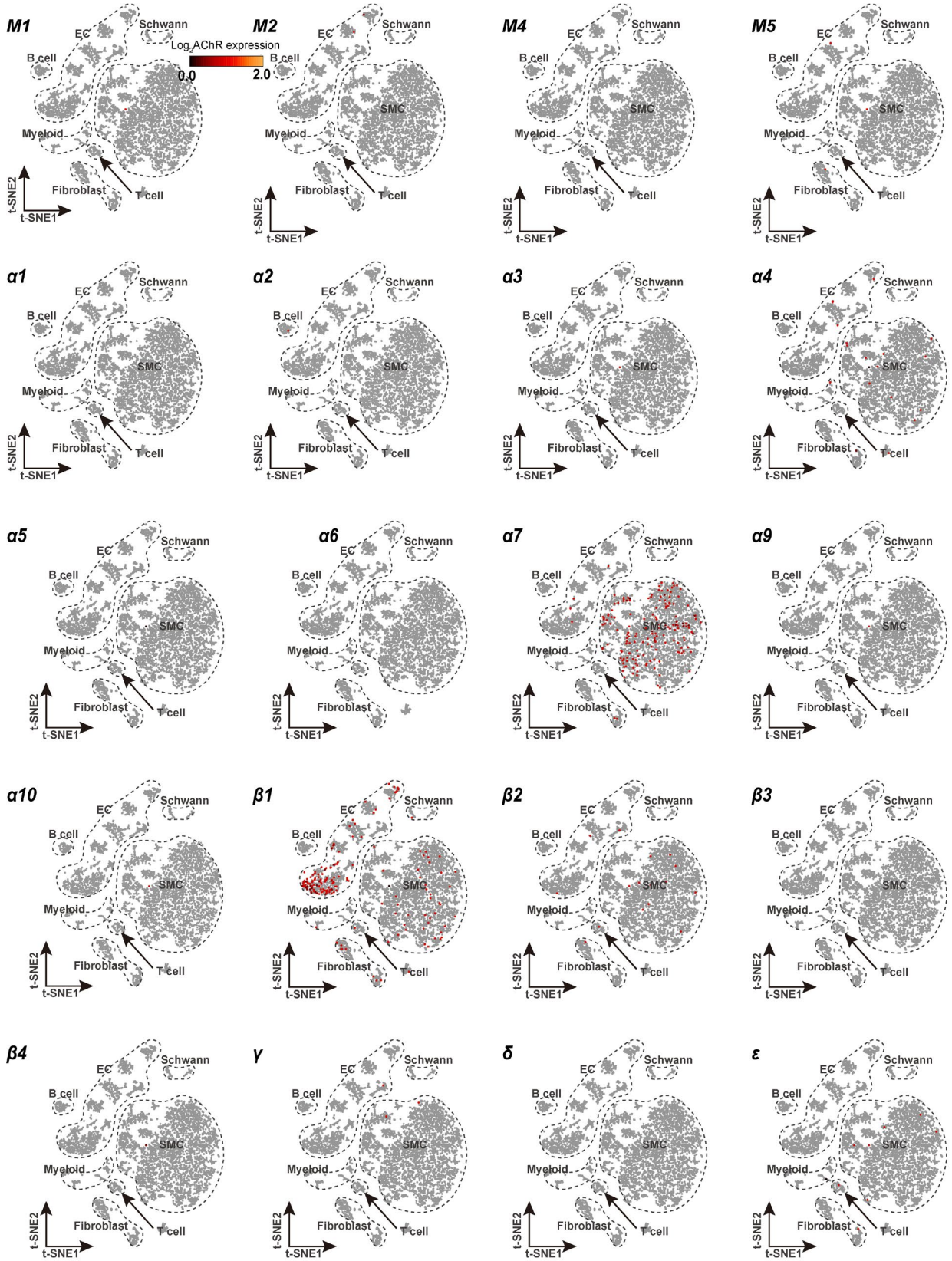

Supplemental Figure 5. Expression of individual *AChRs* in renal artery and its segmental branches. Expression of multiple receptor subtypes were detected in renal arteries and their segmental branches, with higher expression of *nAChRa7* and *nAChRβ1*. T-SNE plots are identical to Figure 5C.

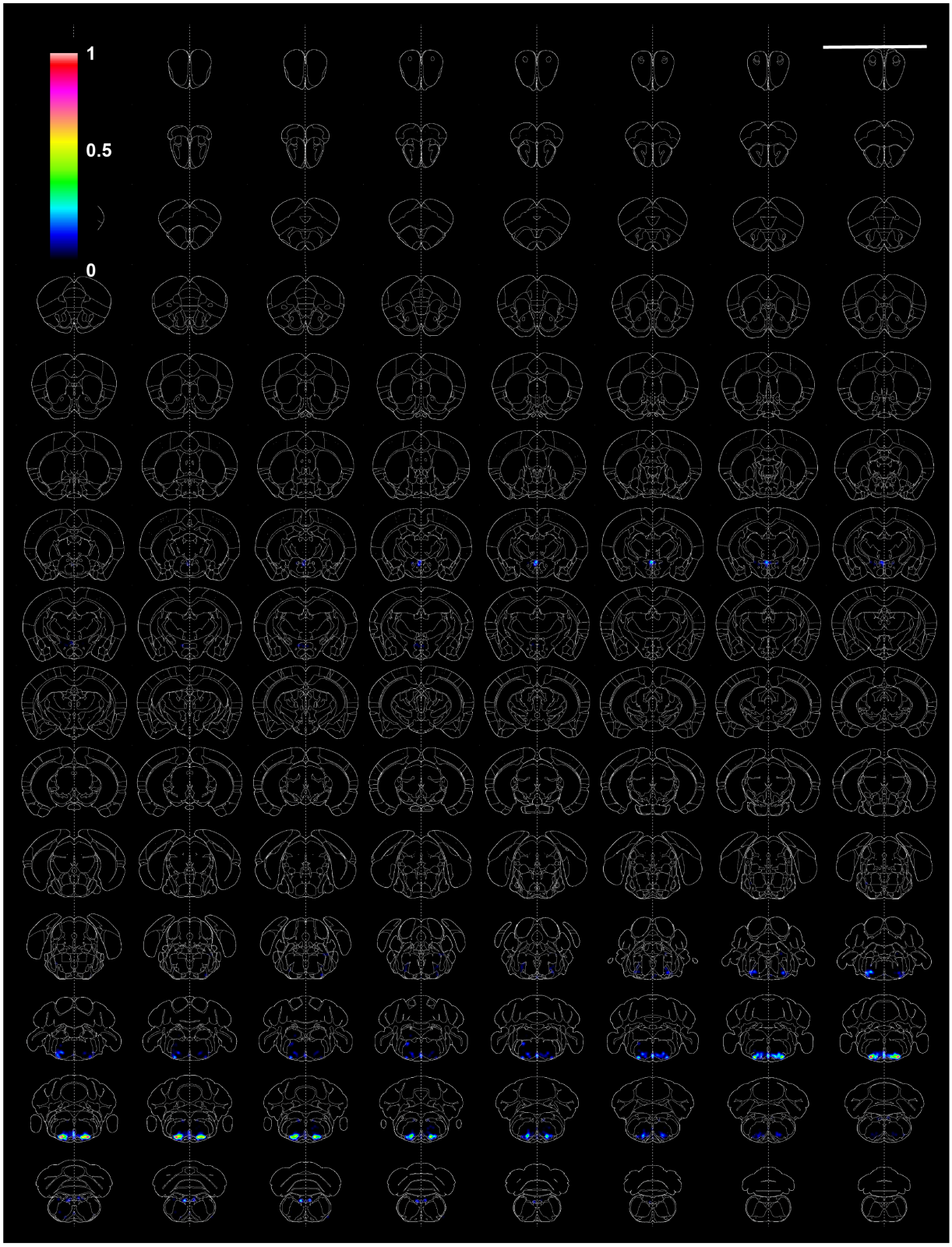

Supplemental Figure 6. Assessment of the synaptic connection between brain and left kidney. Heatmaps of continuous coronal brain slices show the relative distribution density of PRV infected-neurons. The outlines of brain regions were defined according to Allen adult mouse atlas. The interval between coronal slice is 100 μm. Scale bar, 2 cm.

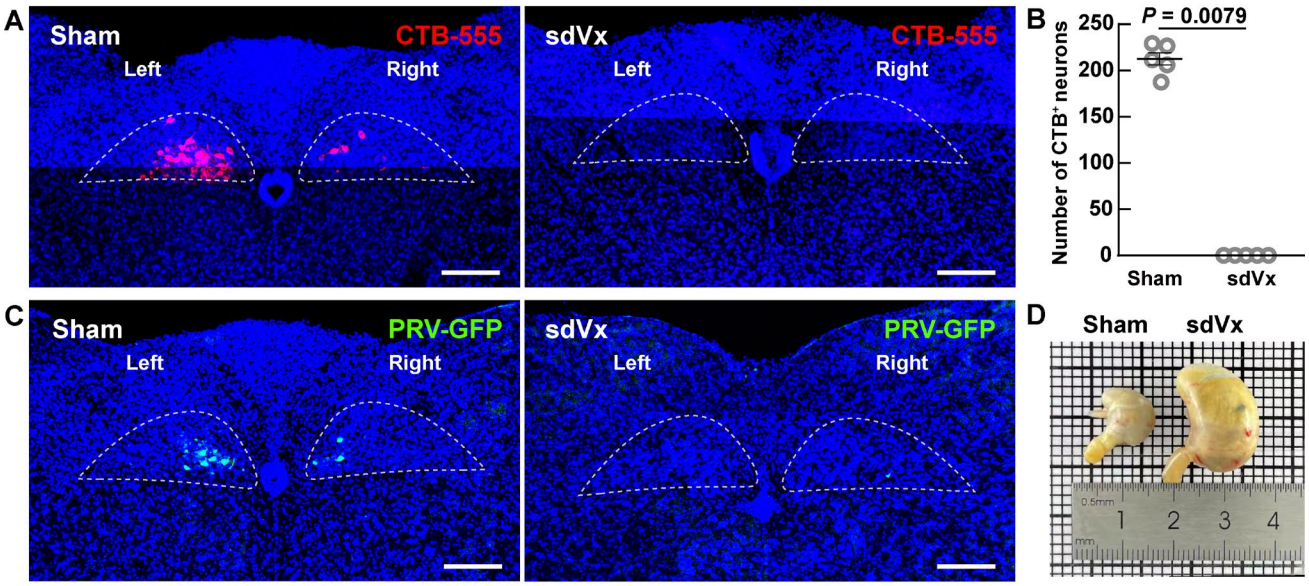

Supplemental Figure 7. CTB and PRV tracing with sdVx. **(A)** CTB-555 labeled neurons (red) in DMX from sham-operated and sdVx mice. Stained with Hoechst 33258 (blue). Scale bars, 200 μm. **(B)** Statistical results for (A) (n = 5 male mice for each group, two-sided Mann-Whitney test, mean ± SEM). **(C)** PRV infected neurons (green) in DMX from sham-operated and sdVx mice. Stained with Hoechst 33258 (blue). Scale bars, 200 μm. Statistical results are shown in Figure 7C. Outlines of the DMX were delineated with dashed lines. **(D)** Anatomical verification of sdVx, showing an enlarged stomach after sdVx. Images representative of n = 5 mice.

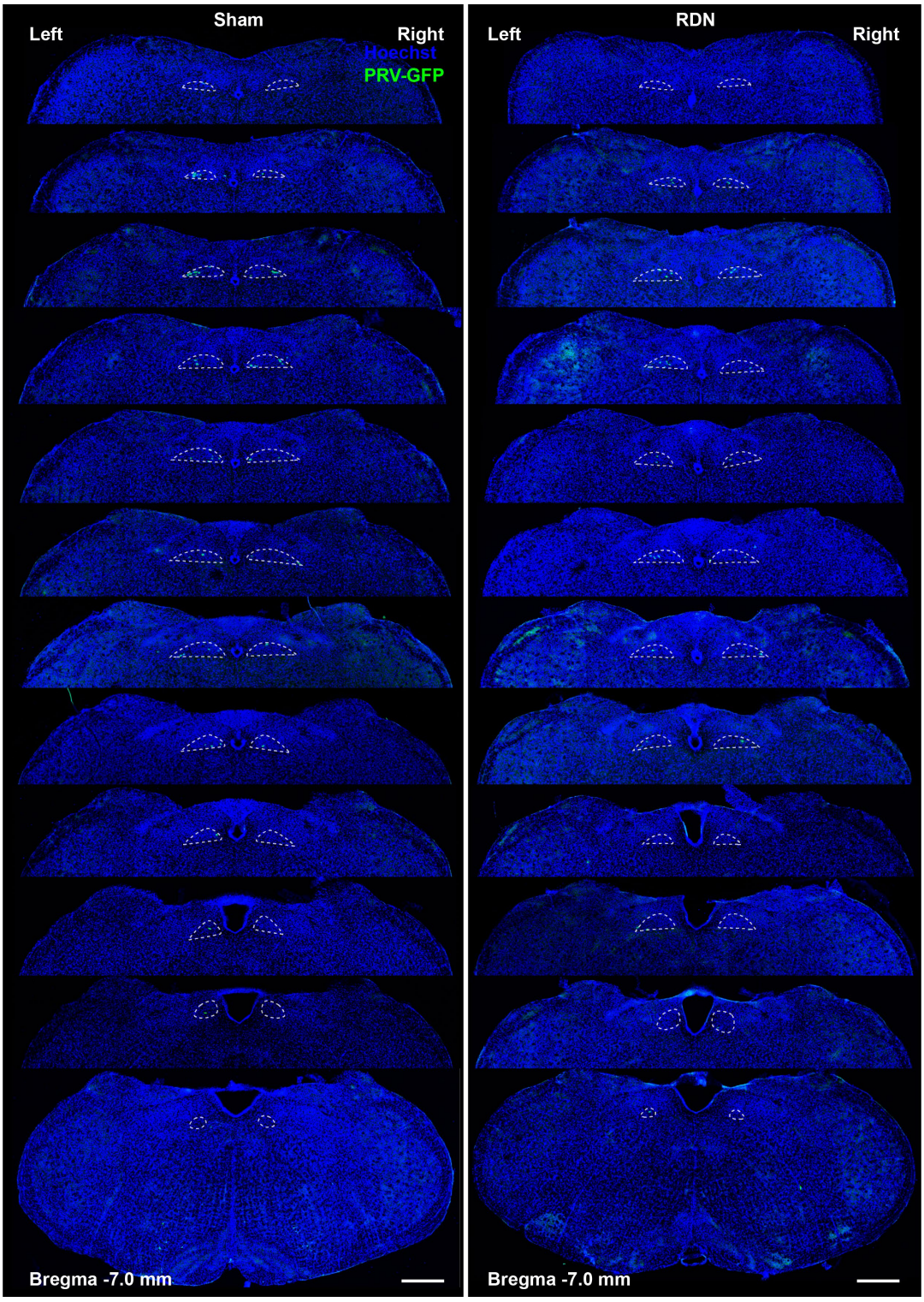

Supplemental Figure 8. Distribution of infected neurons in the DMX after PRV injection. Left sequence: continuous coronal slices from sham-operated mouse brain. Right sequence: continuous coronal slices from renal denervated mouse brain. Neurons infected by PRV were shown in green. Stained with Hoechst 33258 (blue). Outlines of the DMX were delineated with dashed lines. Scale bars, 500 μm.

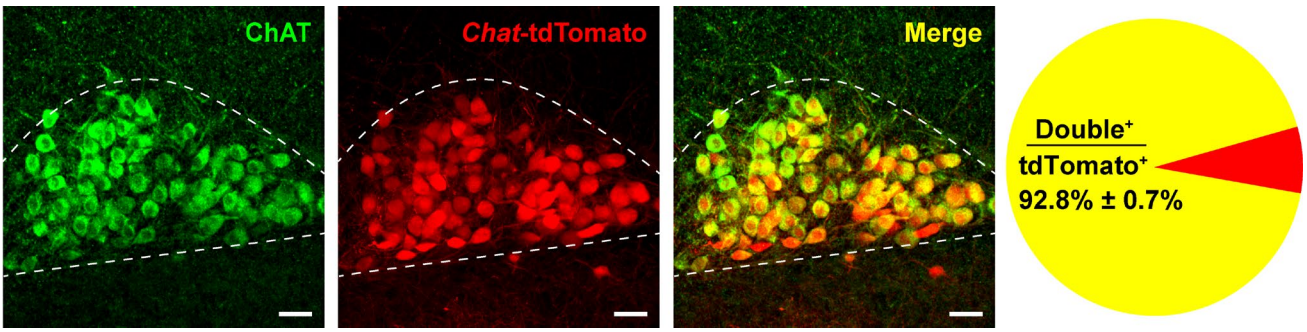

Supplemental Figure 9. Immunostaining indicates that tdTomato expression is faithful to cholinergic neurons in the DMX. Representative images of brain slices from *Chat-ires-Cre*:Ai14 mice, stained for ChAT (green). Dashed lines delineate outlines of the DMX. Scale bars, 50 μm. Statistical result is shown on the right. (n = 3 female mice, mean ± SEM).

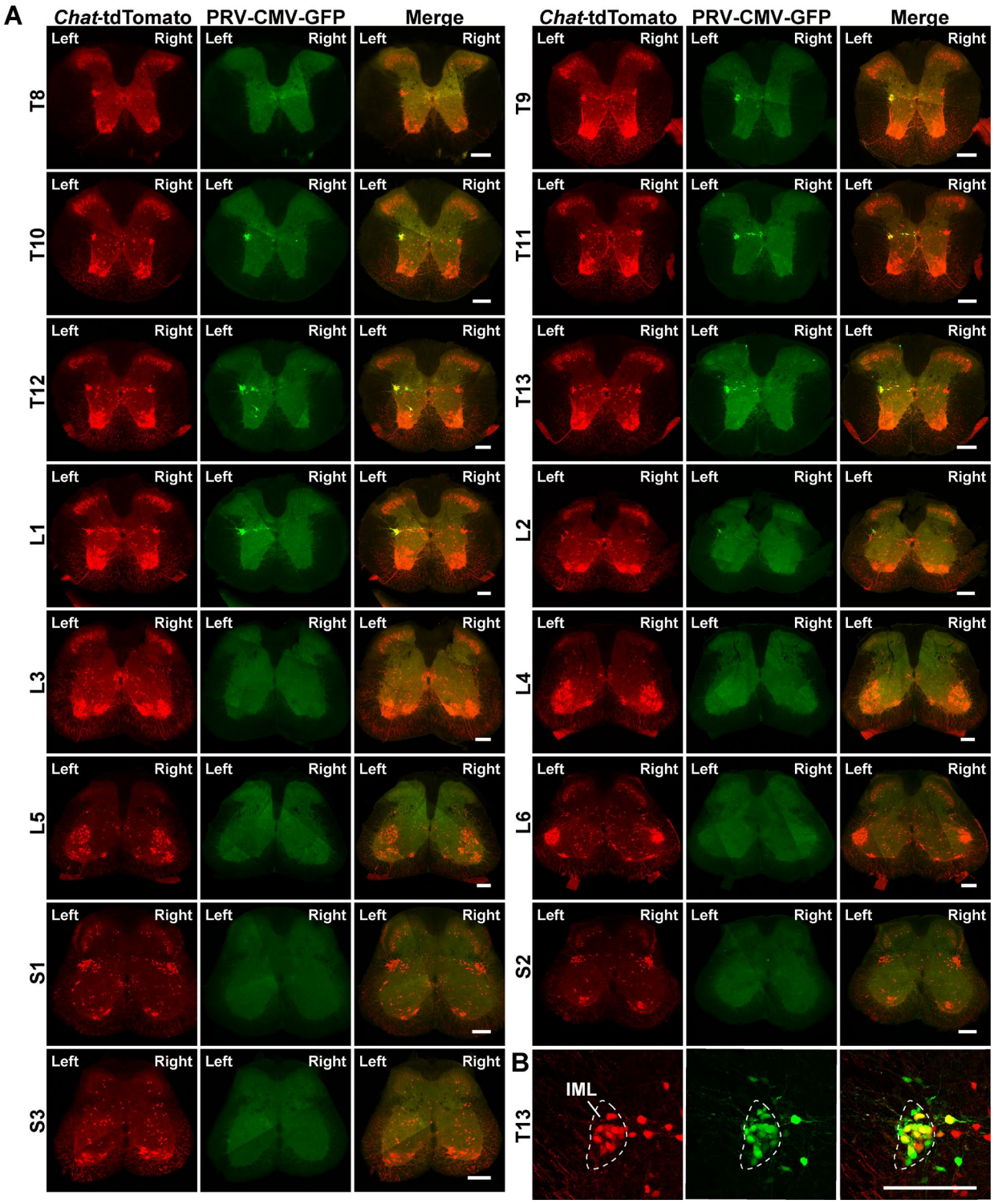

Supplemental Figure 10. Assessment of the synaptic connection between spinal cord and the left kidney. (A) Co-expression profiles of tdTomato (red) and GFP (green) at different spinal cord levels. Note PRV-GFP positive neurons mainly present in the left side and absent in right side. Scale bars, 200 μm. **(B)** Representative images show *Chat*-tdTomato and PRV-GFP double-positive neurons (yellow) in IML of T13. Scale bar, 200 μm.

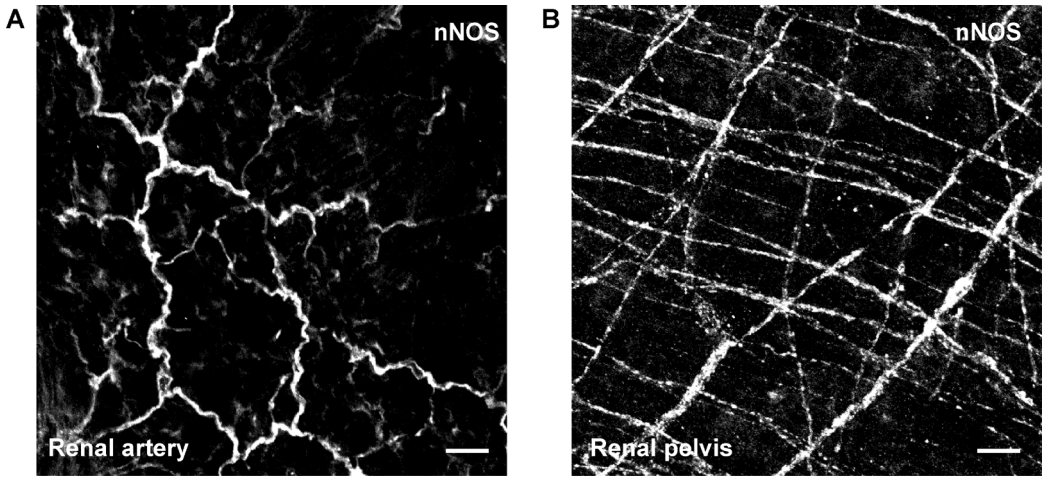

Supplemental Figure 11. Nitrergic nerve fibers associated with the renal artery and pelvic wall of C57BL/6 mouse. (A) Representative image of the renal artery from a C57BL/6J mouse, stained for nNOS (white). Scale bar, 20 μm. **(B)** Representative image of the renal pelvis from a C57BL/6J mouse, stained for nNOS (white). Scale bar, 20 μm.

Supplemental Table 1. Key study purposes, techniques, and mouse strains.

Study Purpose	Technique	Mouse Strain
Identify the cholinergic nerve fibers and ganglion cells around the renal artery.	Immunostaining against ChAT and VAChT for renal arteries.	*Chat-ires-Cre*:Ai14 C57BL/6J
Identify the cholinergic nerve fibers in the renal pelvis wall.	Immunostaining against synapsin for renal pelvises.	*Chat-ires-Cre*:Ai14 C57BL/6J
Identify the cholinergic nerve varicosities that supply the segmental renal artery and renal pelvis.	Immunostaining against synapsin for renal slices and pelvises.	*Chat-ires-Cre*:Ai14
Locate the cholinergic nerve fibers that travel in the rennal pelvis wall.	Dissected out renal pelvises and stained with WGA and Hoechst 33258, followed by three-dimensional imaging.	*Chat-ires-Cre*:Ai14
Evaluate the accuracy of genetic labeling of cholinergic neurons in the DMX of *Chat-ires-Cre*: Ai14 mice.	Immunostaining against ChAT for brain slices.	*Chat-ires-Cre*:Ai14
Evaluate the anatomical relationship between cholinergic and catecholaminergic nerve fibers.	Immunostaining against TH for renal arteries and pelvises.	*Chat-ires-Cre*:Ai14
Evaluate the anatomical relationship between cholinergic and sensory nerve fibers.	Immunostaining against CGRP for renal arteries and pelvises.	*Chat-ires-Cre*:Ai14
Examine the expression of various *AChRs* in renal artery and its segmental branches.	Dissected out renal arteries and segmental renal arteries, followed by scRNA-seq analysis.	C57BL/6J
Confirm the efficacy of RDN.	Established RDN models, followed by immunostaining against TH for renal slices.	C57BL/6J
Confirm the efficacy of sdVx.	Established sdVx models, followed by CTB tracing and stomach anatomy.	C57BL/6J
Establish a control to consider the disturbance from nonspecific AAV spread.	Established RDN models, followed by retrograde AAV tracing	Ai 14
Assess the vagal afferent pathway from kidney to brain.	Retrograde AAV tracing, followed by brain slices and nodose/jugular complexes imaging. Immunostaining against VGluT2 for the nodose/jugular complexes.	Ai 14
Establish a control to consider the disturbance from nonspecific PRV spread.	Established sdVx and RDN models, followed by retrograde PRV tracing.	C57BL/6J
Locate the parasympathetic preganglionic neurons that project to the kidney	Retrograde PRV tracing, followed by whole brain and spinal cord imaging	*Chat-ires-Cre*:Ai14
Identify the nitrergic nerve fibers around the renal artery.	Immunostaining against nNOS for renal arteries.	C57BL/6J

Supplemental Table 2. Primary and secondary antibodies used in this study

Antibodies	Source	Identifier	Specificity
Goat polyclonal anti-ChAT	Millipore	Cat: AB144P, RRID: AB_2079751 Lot: 3067431	Western blotting validation[1, 2]*
Goat polyclonal anti-VAChT	Millipore	Cat: ABN100, RRID: AB_2630394 Lot: 3674955	Western blotting validation[3]
Rabbit polyclonal anti-VAChT	Sigma-Aldrich	Cat: SAB4200559, RRID: AB_2910560 Lot: 099M4867V	Western blotting validation[4]*
Rabbit polyclonal anti-CGRP	Sigma-Aldrich	Cat: C8198, RRID: AB_259091 Lot: 069M4801V	Knockout validation[5]
Rabbit polyclonal anti-TH	Sigma-Aldrich	Cat: T8700, RRID: AB_1080430 Lot: SLCG2110	Western blotting validation*
Rabbit polyclonal anti-Synapsin1	Sigma-Aldrich	Cat: S193, RRID: AB_261457 Lot: MKBZ7798V	Western blotting validation[6]
Rabbit monoclonal anti-nNOS	Abcam	Cat: ab76067, RRID: AB_215246 Lot: GR315913-23	Western blotting validation[7]*
Rabbit monoclonal anti-VGluT2	Abcam	Cat: ab216463, RRID: AB_2893024 Lot:GR3205712-1	Western blotting validation[8]*
Alexa Fluor 488-conjugated goat polyclonal anti-rabbit	Thermo Fisher	Cat: A-11008, RRID: AB_143165 Lot: 1797971	#
Alexa Fluor 488-conjugated donkey polyclonal anti-goat	Thermo Fisher	Cat: A-11055, RRID: AB_2534102 Lot:1942238	#
Alexa Fluor 568-conjugated goat polyclonal anti-rabbit	Thermo Fisher	Cat: A-11036, RRID: AB_10563566 Lot:1504529	#

*Manufacturer's verification.

[#] The specificity was confirmed by the deletion of primary antibody.

Supplemental Table 3. Expression of *AChRs* in renal artery and its segmental branches

Gene symbol	# of log_2Expression>0 cells & % of total[a]						
	SMC	**EC**	**Fibroblast**	**Myeloid**	**Schwann**	**T cell**	**B cell**
mAChR1	—	—	—	—	—	—	—
mAChR2	—	—	—	—	—	—	—
mAChR3	6|<1.0%	172|11.7%	—	1|<1.0%	—	—	1 | <1.0%
mAChR4	—	—	—	—	—	—	—
mAChR5	—	1|<1.0%	1|<1.0%	—	—	—	—
nAChRα1	—	—	—	—	—	—	—
nAChRα2	—	—	—	—	—	—	—
nAChRα3	—	—	—	—	—	—	—
nAChRα4	11|<1.0%	4|<1.0%	1|<1.0%	1|<1.0%	—	—	—
nAChRα5	—	—	—	—	—	—	—
nAChRα6	—	—	—	—	—	—	—
nAChRα7	167|4.3%	4|<1.0%	2|<1.0%	—	—	—	—
nAChRα9	—	—	—	—	—	—	—
nAChRα10	—	—	—	—	—	—	—
nAChRβ1	41|1.1%	130|8.8%	9|2.6%	1|<1.0%	1|<1.0%	1|<1.0%	—
nAChRβ2	10|<1.0%	3|<1.0%	1|<1.0%	—	—	1|<1.0%	—
nAChRβ3	—	—	—	—	—	—	—
nAChRβ4	—	—	—	—	—	—	—
nAChRγ	2|<1.0%	1|<1.0%	—	—	—	—	—
nAChRδ	—	—	—	—	—	—	—
nAChRε	5|<1.0%	—	1|<1.0%	1|<1.0%	—	1|<1.0%	—
Total	363|9.4%	323|21.9%	40|11.7%	5|2.2%	3|2.6%	4|3.6%	1|<1.0%

[a]Dashes indicate no elements found in scRNA-Seq.

Reference

1. Nango H, Kosuge Y, Sato M, Shibukawa Y, Aono Y, Saigusa T, et al.: Highly Efficient Conversion of Motor Neuron-Like NSC-34 Cells into Functional Motor Neurons by Prostaglandin E_2. *Cells,* 9: 1741, 2020
2. Martinelli I, Tayebati SK, Roy P, Micioni Di Bonaventura MV, Moruzzi M, Cifani C, et al.: Obesity-Related Brain Cholinergic System Impairment in High-Fat-Diet-Fed Rats. *Nutrients,* 14: 1243, 2022
3. Vetreno RP, Broadwater M, Liu W, Spear LP, Crews FT: Adolescent, but not adult, binge ethanol exposure leads to persistent global reductions of choline acetyltransferase expressing neurons in brain. *PLoS One,* 9: e113421, 2014
4. Elwary SM, Chavan B, Schallreuter KU: The vesicular acetylcholine transporter is present in melanocytes and keratinocytes in the human epidermis. *J Invest Dermatol,* 126: 1879-1884, 2006
5. Ishida K, Kawamata T, Tanaka S, Shindo T, Kawamata M: Calcitonin gene-related peptide is involved in inflammatory pain but not in postoperative pain. *Anesthesiology,* 121: 1068-1079, 2014
6. Frederikse PH, Yun E, Kao HT, Zigler JS, Jr., Sun Q, Qazi AS: Synapsin and synaptic vesicle protein expression during embryonic and post-natal lens fiber cell differentiation. *Mol Vis,* 10: 794-804, 2004
7. Tan M, Yang T, Liu H, Xiao L, Li C, Zhu J, et al.: Maternal vitamin A deficiency impairs cholinergic and nitrergic neurons, leading to gastrointestinal dysfunction in rat offspring via RARbeta. *Life Sci,* 264: 118688, 2021
8. Zhang H, Zou Y, Lei H: Regional metabolic differences in rat prefrontal cortex measured with in vivo ^{1}H-MRS correlate with regional histochemical differences. *NMR Biomed,* 32: e4024, 2019